3. R. K. Penny and D. R. Hayhurst, "The deformations and stresses in a stretched thin plate containing a hole during stress redistribution caused by creep," Int. J. Mech. Sci., 11, No. 1 (1969).
4. K. M. Manukyan, V. M. Morozov, and V. T. Sapunov, "Calculating creep in construction elements by the finite element method," Prikl. Mekh., 20, No. 11 (1984).
5. Yu. N. Shevchenko and V. N. Mazur, "Solution of planar and axisymmetric boundary problems of thermoviscoplasticity with consideration of material degradation from creep," Prikl. Mekh., 22, No. 5 (1986).
6. D. R. Hayhurst, P. R. Dimmer, and M. W. Chernuka, "Estimates of the creep rupture lifetime of structures using the finite element method," J. Mech. Phys. Solids, 23, No. 4/5 (1975).
7. G. S. Lee and L. C. Smith, "Analysis of a power-law material containing a single hole subjected to a uniaxial tensile stress using the complex pseudo-stress function," Trans. ASME: J. Appl. Mech., 55, No. 2 (1988).
8. J. Boyle and J. Spence, Stress Analysis in Structures with Creep [Russian translation], Mir, Moscow (1986).
9. K. Yu. Bate and E. L. Wilson, Numerical Analysis Methods and the Finite ELement Method [in Russian], Stroiizdat, Moscow (1982).
10. D. K. Fadeeev and V. N. Fadeeva, Linear Algebra Calculation Methods [in Russian], Fizmatgiz, Leningrad–Moscow (1963).
11. A. Durelli and V. Parks, Moire Analysis of Strain, Prentice-Hall, NJ (1971).
12. V. A. Zhilkin and A. M. Popov, "Study of elastoplastic deformations," Zavod. Lab., 53, No. 9 (1987).

FRACTURE FAILURE IN THE ALLOY AMg6

S. A. Novikov and A. I. Ruzanov

UDC 539.4

Fracture failure in construction materials is preceded by stages of generation, growth, and merger of microcracks of micropores. Studies of the kinetics of fracture formation under dynamic loading resulting from an intense blow on the specimen or its rapid heating have been given a great deal of attention by theoreticians and experimenters. It is well known that the character of failure and the value of fracture strength depend significantly on loading conditions, and the original state of the material. As a rule, generation of microfissures occurs in regions where microstructural defects are located. A promising direction in the study of dynamic failure processes is numerical computer experiment, performed using results of physical experiments. With a proper choice of failure model which considers the real process of fracture formation, such studies permit more detailed clarification of the features of failure.

The present study will offer results of studies in the above direction regarding fracture failure of the aluminum alloy AMg6. This alloy is one of the most widely used materials in modern technology designs, including those used under conditions of intense dynamic loading at elevated temperature. A number of studies have considered its strength characteristics under shock wave loading experimentally (see [1-3] and bibliography therein). In the experiments, results of which were used in the present study for numerical modeling of the fracture failure process, the specimens (80 mm diameter disks 10 mm thick) were loaded by impact of an aluminum plate 4 mm thick, driven to a specified velocity by a sheet charge of explosive material. A portion of the specimens studied were used as supplied (rolled), while a portion were annealed at 320°C for 1 h. Specimens were heated before loading with a radiant heater. After loading, sections were cut from the specimens for metallographic analysis at a magnification of 1000 times. Typical photographs of AMg6 specimen microstructure in the failure generation zone are shown in Fig. 1 (a, temperture 0°C, b, 550°C). Over the entire temperature range generation of microfissures occurred at accumulations of inclusions extended in the direction of rolling. At elevated temperatures merging of the cavities formed occurred primarily in a direction perpendicular to the rolling direction. Cracking along

Moscow. Translated from Zhurnal Prikladnoi Mekhaniki i Tekhnicheskoi Fiziki, No. 2, pp. 158-162, March-April, 1991. Original article submitted March 7, 1989; revision submitted October 10, 1989.

 0021-8944/91/3202-0288$12.50

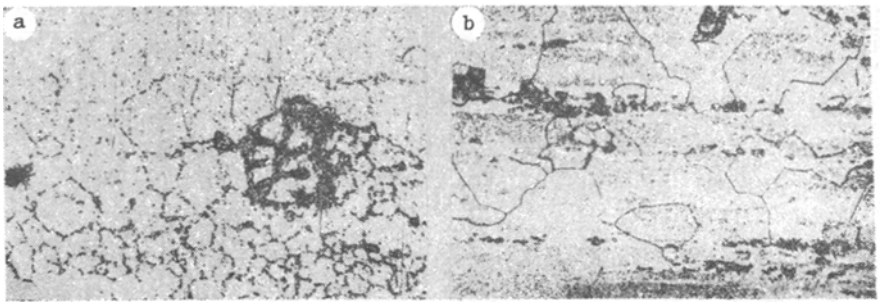

Fig. 1

fine grain boundaries was also observed.

Some experimental results are also presented in Tables 1 and 2 for unannealed and annealed specimens, respectively. The degree of damage in the specimens was characterized using the following notation [3]: A, absence of microdamage in the section when observed at 1000 times magnification; B, presence in the fracture zone of individual isolated microfailures, observed under the microscope; C, intense microfailure of material (significant number of isolated and merged microfailures observed under the microscope); D, slight macrofailure of the specimen (presence in the fracture zone of small macrocracks, observable visually in an etched section); E, partial fracture failure (individual sections of major crack in section); F, complete fracture failure (main fracture crack passing through entire specimen section visible).

Numerical modeling with a computer was then used to study further fracture failure processes in the same specimens at normal temperature. The mechanical arrangement of the experiment was described above, and collision conditions are given in Tables 1 and 2. The mathematical formulation of the problem, the system of differential equations, failure model, and equations of state of the medium used in the numerical experiments were presented in detail in [4]. We will note that in the calculations fracture failure was described as a process of formation, growth, and merger of pores, and the relative pore volume [4] was used as a measure of degradation. This model corresponds to the character of fracture failure of the specimens observed in physical experiment. Estimates of the applicability of this model were carried out previously (see [4, 5] and bibliography therein) by comparing numerical results with experimental data and calculations of other authors. Dynamic fracture failure was considered over a wide range of collision velocities, striker and target thicknesses, and various materials. Calculation results were compared with experiment using a wide range of parameters: relative cavity volume distribution over thickness, location and size of damaged regions within the specimens, free surface motion velocity profiles. The numerical results evaluated below were obtained using the following data for AMg6 specimens in the rolled state: density $\rho_0 = 2.71$ g/cm^3, shear modulus G = 27.7 GPa, volume compression modulus K = 72.8 GPa, yield point $\sigma_t = 0.26$ GPa; the constants used to describe the failure process were: $\sigma_{n0} = 0.3$ GPa, $\sigma_{g0} = 0.4$ GPa, $R_0 = 10^{-4}$ cm, $\sigma_I = 0.04$ GPa, $\eta = 20$ Pa·sec. Results are presented in Table 1 and Figs. 2 and 3. In Table 1 W_0 indicates the velocity of the striker plate, σ_- is the compressive stress impulse, σ_+ is the maximum value of tensile stress in the fracture plane, and V_p is the relative pore volume in the fracture plane. In Fig. 2 the abscissa represents time while the ordinate is the velocity of the free target surface; Fig. 3 shows the change with time of the volume fraction of cavities and stresses for various collision velocities, while Figs. 4, 5 and Table 2 are changes in the same quantities for specimens subjected to annealing. Curve numbers correspond to the variant numbers in the tables. In the stress–time curves the elastic precursor is not shown. Annealing is as a rule used to relieve internal stresses, and leads to a more uniform distribution of intermetallic inclusions. One of the mechanical manifestations of annealing is a reduction in the yield point. In connection with this calculations for the annealed specimens were performed with the same physicomechanical characteristics as indicated above, but with the yield point at 0.16 GPa [3]. Comparing Tables 1 and 2, we see that in the annealed specimens creation of the same degree of damage requires significantly less collision velocity. In partiuclar, for rolled specimens with a collision velocity $W_0 = 190$ m/sec $V_p = 0.143$, while for annealed specimens at $W_0 = 175$ m/sec $V_p = 0.26$. To study this factor in grater detail numerical calculations were carried out for an annealed specimen with $W_0 = 380$ m/sec and compared with variant 6 of Table 1. The velocity of the back free target surface for this case is shown by the crosses of

TABLE 1

Variant number	W_0, m/sec	σ_-, GPa	σ_+, GPa	V_p
1 (A)	141	1,06	0,93	$6,4 \cdot 10^{-3}$
2 (B)	155	1.15	0,96	$2,1 \cdot 10^{-2}$
3 (C)	190	1,4	1,15	0,143
4 (D)	296	2,23	1,05	0,43
5 (D)	331	2,5	0,97	0,486
6 (E)	380	2,8	1,1	>0,56
7 (F)	410	3,0	1,2	>0,63

TABLE 2

Variant number	W_0, m/sec	σ_-, GPa	σ_+, GPa	V_p
1 (A)	80	0,6	0,52	10^{-8}
2 (B)	105	0,77	0,68	$1,2 \cdot 10^{-3}$
3	140	1,02	0,89	$4,3 \cdot 10^{-2}$
4 (E)	175	1,27	1,05	0,26
5 (E)	210	1,5	1,09	0,39
6 (F)	254	1,8	1,1	>0,46

Fig. 2, while the stresses σ_- were almost identical and equal to 2.74 GPa, $\sigma_+ = 0.84$ GPa, $V_p > 0.73$.

As is well known, the change in velocity of the specimen free surface as compared to its motion in the absence of failure is caused by propagation of a disturbance formed in the growing pore zone. In connection with this the fracture strength is often determined by the difference of the maximum and minimum (value at the first minimum) of the free surface velocities, $\sigma_* = 0.5\rho_0 c_0 (W_1 - W_2)$. Values of σ_* calculated with this expression for curves 3, 6, and the curve represented by the crosses of Fig. 2, i.e., for unannealed and annealed specimens, were 1.06 and 0.83 GPa, respectively. As is evident, these differ by approximately 25%. Significant reduction in fracture strength upon annealing (up to 30%) was observed in the experimental studies [1-3].

Naturally the results obtained do not explain all aspects of the matter, and clarification of the effect of annealing on strength and other characteristics will require further studies.

The deformation rate in the failure zone during compression and expansion is of definite interest, since some data indicate that the former effects the strength properties of the material, and in the final reckoning, the failure process. The calculations performed yielded the following results: for $W_0 = 80$ m/sec in the compression wave $\dot{\varepsilon}$ reached $3.3 \cdot 10^4$ sec^{-1}, and $3.9 \cdot 10^4$ sec^{-1} during expansion, at $W_0 = 141$ m/sec $\dot{\varepsilon} = 4.6 \cdot 10^4$ and $7.6 \cdot 10^4$ sec^{-1}, at $W_0 = 296$ m/sec $\dot{\varepsilon} = 1.6 \cdot 10^5$ and $3.4 \cdot 10^5$ sec^{-1}, and at $W_0 = 410$ m/sec $\dot{\varepsilon} = 2 \cdot 10^5$ and $5 \cdot 10^5$ sec^{-1}, respectively. From this it is evident that in the collision velocity range considered $\dot{\varepsilon}$ changes by a full order of magnitude and the process of damage formation and growth leads to a significant increase in the deformation rate.

It follows from the results presented that formation and growth of micropores leads to a significant change in the stress field within the specimen, which in turn has an effect on failure kinetics, leading to a change in velocity of the specimen free surface. For significant degrees of damage the effects of these processes, in particular, relaxation of tensile stresses due to formation and growth of pores, manifest themselves to a large degree, and in this case there is a certain clarity to the situation. There has not been enough study of the effects of damage in the early stages of fracture failure – in the prefracture stage in the terminology of [6] (see variants 1-3 in Tables 1, 2). As is evident from W(t) and σ(t) curves, damage up to several percent (to 4% in an annealed specimen, 2% in the unannealed) has practically no effect on the stress and deformation field. At high V_p levels the σ(t) and W(t) profiles differ markedly from corresponding ones without consideration of damage. Then, admittedly with a certain arbitrariness, we can find some threshold collision velocity, which when exceeded slightly leads to marked (almost avalanche-like) increase in damage. For the variants considered this would be a collision velocity of about 155 m/sec for unannealed and 140 m/sec for annealed specimens (see Tables 1, 2). These results agree qualitatively with the experimental data of [3, 7] on dependence on collision velocity of residual strength and total crack length, used in [6, 7] as a measure of damage, some justification of which can be found by analyzing the distribution of relative pore volume over specimen thickness. Such a dependence is shown in Fig. 6 for $W_0 = 190$, 296, and 410 m/sec (curves 1-3). For the last variant only the upper part of the distribution is shown, since at low damage levels curves 2 and 3 are similar. In the calculations shown merger of micropores within the calculation cell was not considered, and relative pore volume could grow without limit up a value of unity. It follows from Fig. 6 that pores are formed in a large number of elements and that this region encompasses half the specimen thickness, although the most significant pores occur in a narrow zone, where formation of the main crack occurs. On this subject we

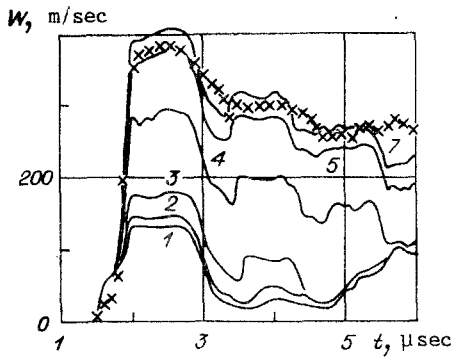

Fig. 2

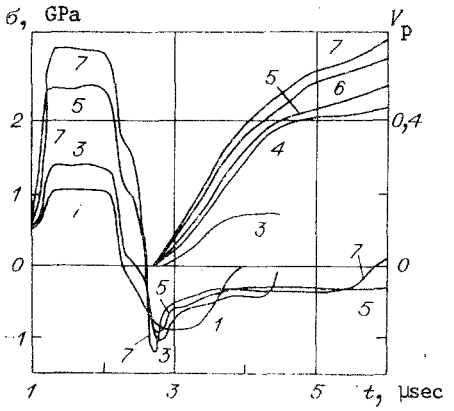

Fig. 3

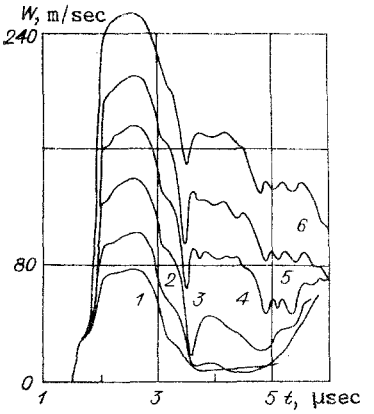

Fig. 4

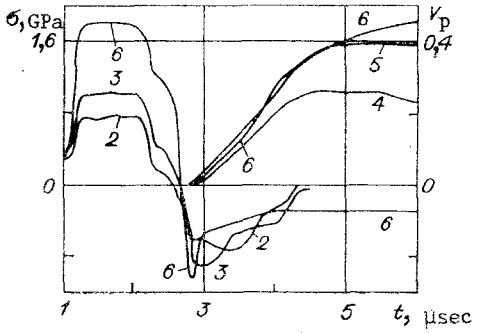

Fig. 5

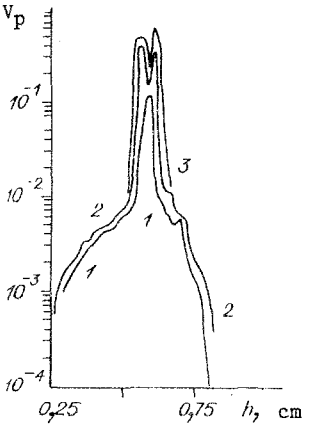

Fig. 6

will note that with increase in W_0 that damage in the low level areas increases only insignificantly, while there is marked growth in just that narrow zone noted above, i.e., the failure process becomes localized. With increase in W_0 the character of the relative pore volume distribution over specimen thickness also changes: it has the form of a curve with two maxima and a drop between (see Fig. 6). Such a configuration is formed only for sufficiently high collision velocities: for unannealed specimens at $W_0 \geqslant 296$ m/sec, and for annealed ones at $W_0 > 254$ m/sec. In these cases the amount of damage exceeds 40% and the failure process apparently transforms into its final stage.

On the whole it can be stated that all the features described above apparently correspond to various stages of fracture failure, and the corresponding values of collision velocity, stress, and damage distinguish one stage from the other.

LITERATURE CITED

1. S. A. Novikov, "Strength in quasistatic and shock wave loading," Fiz. Goreniya Vzryva, No. 6 (1985).
2. V. K. Golubev, S. A. Novikov, Yu. S. Sobolev, et al., "Character of fracture failure of aluminum and its alloys D16 and AMg6 in the temperature range −196-600°C," Probl. Prochn., No. 2 (1983).
3. V. K. Golubev, A. I. Korshunov, S. A. Novikov, et al., "Strength and failure of the aluminum alloy AMg6 under shock wave loading," Zh. Prikl. Mekh. Tekh. Fiz., No. 2 (1988).
4. A. I. Ruzanov, "Numerical study of fracture strength with consideration of micro-degradation," Izv. Akad. Nauk SSSR, Mekh. Tverd. Tela, No. 5 (1984).
5. A. I. Ruzanov, "Study of dynamic fracture failure in unloading waves," Izv. Akad. Nauk SSSR, Mekh. Tverd. Tela, No. 2 (1985).
6. V. I. Romanchenko, "Aluminum alloy failure in the prefracture stage," Probl. Prochn., No. 6 (1983).
7. V. I. Romanchenko, O. I. Marusii, and I. V. Kramarenko, "Microstructure of aluminum alloy in the early stages of fracture," Probl. Prochn., No. 9 (1983).